UNISeC: Inspection, Separation, and Classification of Underwater Acoustic Noise Point Sources

Mehdi Rahmati, Student Member, IEEE, and Dario Pompili, Senior Member, IEEE

Abstract-Advancements in oceanic research have resulted in a plethora of activities such as undersea oil/gas exploration, environmental monitoring, sonar-based coastal surveillance, which have each increased the acoustic noise levels in the ocean and have raised concerns in the scientific community about the effect of human-generated sounds on marine life. Knowledge of the statistical characteristics of noise sources and their spatial distribution is paramount for understanding the impact on marine life as well as for regulating and policing such activities. Furthermore, studies have shown that assuming the underwater noise probability density function to be Gaussian, exponential, or Weibull is often not valid; therefore, statistically profiling the sources of the ambient noise is also essential to improve the performance of acoustic communication systems in the harsh underwater environment. In this paper, a novel solution based on the blind source separation method is proposed to enable separation of underwater acoustic noise point sources in the presence of channel propagation multipath. The proposed Underwater Noise Inspection, Separation, and Classification (UNISeC) system performs several pre- and postprocessing steps forming a novel gray-box model. Assuming there is no prior information on the noise sources, UNISeC estimates the number of such sources as well as characterizes and classifies them via a recursive pilot-aided probing method while minimizing the environmental acoustic contamination. A correlation-based characterization as well as power spectral density based classification approaches are investigated to verify the proposed method. Several scenarios are also presented and evaluated in detail via simulations.

Index Terms—Blind source separation (BSS), point sources, system modeling, underwater acoustic noise, underwater acoustic channel propagation.

I. INTRODUCTION

VER the past few years, underwater acoustic communications and networks comprising static sensors as well as mobile vehicles have attracted the attention of both researchers and engineers because they enable a wide variety of applications. There is an increasing interest in applications such as undersea oil/gas exploration, environmental monitoring, and coastal surveillance [2], [3]. All these activities contribute significantly to the underwater acoustic noise, as depicted in Fig. 1: e.g., shipping noise is generated from cargo vessel

Manuscript received June 30, 2016; revised December 4, 2016 and February 13, 2017; accepted July 10, 2017. This work was supported by the NSF CA-REER Award OCI-1054234. This paper was presented in part at the 2014 IEEE Underwater Communications Networks, La Spezia, Italy, Sep. 3–5, 2014 [1]. (Corresponding author: Mehdi Rahmati.)

Associate Editor: L. Culver.

The authors are with the Department of Electrical and Computer Engineering, Rutgers University, New Brunswick, NJ 08901 USA (e-mail: mehdi_rahmati@cac.rutgers.edu; pompili@cac.rutgers.edu).

Digital Object Identifier 10.1109/JOE.2017.2731061

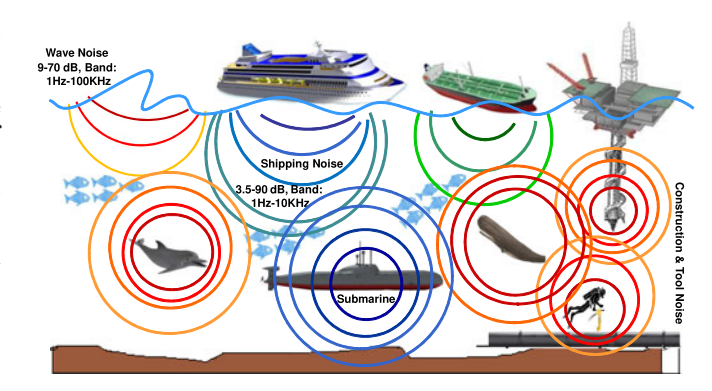


Fig. 1. Example of underwater dominant man-made and natural acoustic noise sources such as ships, undersea exploration and construction, and their effects on marine life.

engines; drilling/extraction noise is produced by airgun arrays, which are used to detect oil/natural gas beneath the seafloor; sonar noise is generated from oceanic acoustic tomography, prospection, and military systems to detect submarines.

Recently, deep-sea audio recording by researchers in the National Oceanic and Atmospheric Administration and their partners has revealed that the ocean is not quiet. Instead of finding silence, even the deepest part of the world's ocean, at the bottom of the Mariana Trench¹ with a depth of more than 36 000 ft, is an incredibly noisy place [4]. Shallow water and coastal regions are also not noise free and are occupied with several noise sources such as impulsive colored noise created by large populaces of snapping shrimp inhabiting these regions [5]. Generally, two main categories of noise sources can be recognized: natural and anthropogenic sources. Natural noise is a phenomenon already present in the environment and marine animals are almost adapted to it; however, its effect on marine mammals can be investigated. Sources such as seismic [6], wave, and rain are often high power and occupy the same frequency band as those used by marine animals, as reported in Figs. 2 and 6. Therefore, they sometimes cause trouble for animals to communicate and estimate distances. On the other hand, human-generated noise sources, such as shipping, drilling and explosions, sonar systems, etc., threaten the animals living in the ocean where it is difficult to distinguish them from natural sounds leading to accidental collisions and mass beachings. Other impacts include causing animals to alter their behavior, preventing them from

¹The Mariana Trench is located in the western Pacific Ocean, to the east of the Mariana Islands.

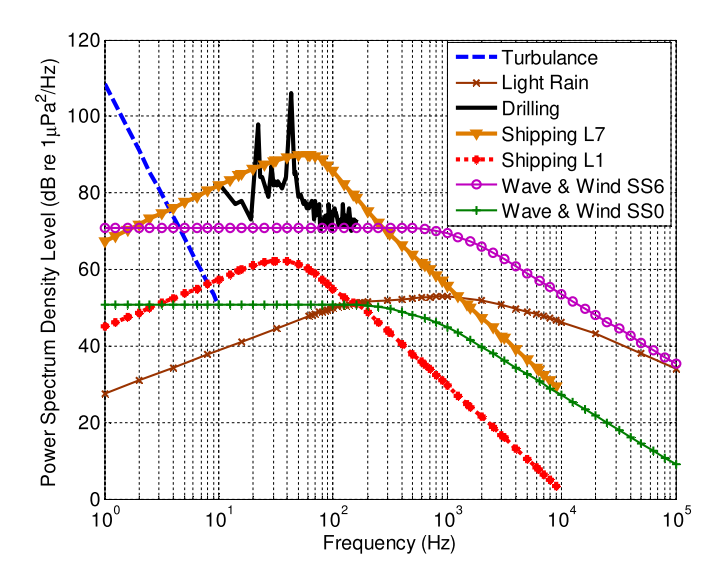


Fig. 2. PSD of acoustic noise sources—as reported in [8, pp. 132–137], [9]—and levels of shipping noise (L1–L7) based on shipping traffic/activities and on the sea states (SS).

hearing important sounds (masking), causing hearing loss (either temporary or permanent), or damaging tissue. In at least a few well-documented cases, a relationship was shown between the use of midfrequency sonar and the stranding of cetaceans, particularly beaked whales [7]. As a result, there are raising concerns in the scientific community about the effect of humangenerated and natural sounds on marine life, which has become a topic of increasing controversy, especially regarding marine mammals.

Knowledge of the statistical characteristics of these noise sources and their spatial distribution is important for better understanding the impact on marine life as well as for regulating and policing shipping and undersea activities—both civilian and military. Furthermore, profiling (e.g., via separation, classification, and statistical analysis) of the dominant sources forming the ambient noise is also essential to increase the performance of acoustic communication systems in the harsh underwater environment. Typically, in the presence of noise and interference, signal-detection performance of communication systems degrades [10], and the problem becomes more severe and complex to compensate for when the noise distribution is not known. Data-driven studies have shown that the assumption of noise to be additive Gaussian is often invalid in ocean environments [11], [12]. In this unfavorable condition, the received signal is mixed with the ambient noise with an unknown distribution, leading to poor performance when traditional reception techniques assuming additive Gaussian noise are adopted.

In Fig. 3, we provide probability plots of the noise data set obtained from $in\ situ$ measurements [8] that are used to evaluate whether such noise data follow regular distributions. This data set is plotted against theoretical normal, exponential, and Weibull distributions such that the output is a straight line and well placed on the reference line if it fits those distributions. In this method, the ith-ordered sample value of a sequence with n samples is sketched against the empirical

cumulative density function on the y-axis, which corresponds to (i-0.5)/n of the ith-ordered sample value. This midpoint probability plotting position method follows the Hazen formula [13]; note that by subtracting 0.5 from the sample, it is ensured that it is exactly in the middle of the interval [(i-1)/n, i/n]. As shown, a deviation from the considered distributions is obvious given the apparent departure from the straight reference line. This confirms empirically that the three noise sources considered (i.e., shipping, wave, and rain noise) cannot be modeled using simplistic known distributions because their statistical deviations (in the center or in the tails) are not negligible.

In this paper, to catch "on the fly" unknown noise sources in the presence of multipath in a three-dimensional (3-D) scenario, we utilize blind source separation (BSS). The proposed system, called Underwater Noise Inspection, Separation, and Classification (UNISeC), is based on BSS and performs preand postprocessing analyses that are specifically designed for the underwater multipath environment. We present a least contaminant pilot-aided probing method to identify the number of dominant sources in each frequency subband, a separation method, and afterward the characterization of the sources based on their magnitude squared coherence estimate (MSCE) and maximum cross correlation (MCC). Finally, we classify them via the coherence of their estimated power spectral density (PSD) and the PSD of known noise sources. Furthermore, regarding unknown distributions of noise sources, several scenarios are considered to evaluate the performance of the proposed system. Simulations show the effectiveness of the proposed solution under various levels of multipath in the ocean.

The remainder of the paper is organized as follows. In Section II, we provide the necessary background and discuss the related work. In Section III, we focus on the problem definition and describe our solution in the context of a system named UNISeC. In Section IV, we present performance evaluations and discuss the obtained results. Finally, in Section V, we conclude this paper.

II. BACKGROUND AND RELATED WORK

A. Underwater Noise Pollution and Marine Mammal Protection

The emerging trend of underwater noise level due to marine industry leads to more noise pollution and increasingly threatens the marine life. Many countries and oceanic regions have recognized the need to establish rules for policing the spectrum underwater. Several experiments confirm that man-made noise such as sonar is harmful to marine mammals, especially for blue and beaked whales [14]. In [15], the propagation of underwater noise, especially from ships, is modeled and the received levels by species-specific audiograms are analyzed. *In situ* measurements of underwater noise are critical for the assessment of risk to marine life. In [16], guidance is provided for *in situ* measurement of underwater sound using several metrics. Real-world data can be used in passive acoustic tomography [17], which leads to a promising way to reduce acoustic emissions in the

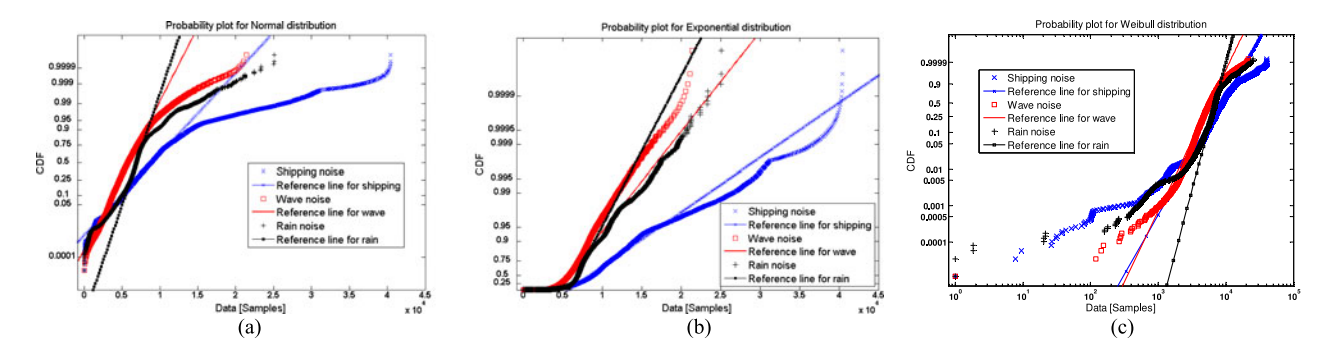


Fig. 3. Statistical deviation of noise sources from (a) normal, (b) exponential, and (c) Weibull distributions. Reference lines compare the distribution of the data against these three known distributions. Noise data were obtained from [8, pp. 132–137].

oceans. Acoustic tomography has been considered for several studies in shallow- and deep-water research [18]; however, more serious actions are required before this problem turns into an environmental crisis.

B. Spectrum Sensing, Ocean Monitoring/Policing

Spectrum sensing is the first step for using the acoustic spectrum more efficiently. This procedure is performed by listening and obtaining knowledge on the spectrum usage as well as on the presence or absence of primary users in predefined frequency subbands. It is the most important part of a cognitive radio structure in terrestrial scenarios. In [19], its concepts, methodologies, and challenges have been discussed. Energy-detection sensing, matched filtering, and cyclostationary feature detection are three common techniques used to improve the spectrum sensing process [20]. Baldo et al. [21] applied cognitive radio and a dynamic spectrum access method to the underwater environment. In [22], an underwater acoustic recording has been implemented as a solution for monitoring disturbance reactions of marine mammals. To our knowledge, there is no comprehensive and systematic research on how to effectively monitor and police the ocean noise in the literature. The proposed work plan intends to cover this gap.

C. Blind Signal Separation

BSS solves the problem of source recovering from the observation of their mixtures at the receivers without any knowledge about the mixing coefficients. It has been widely considered by the researchers in various applications such as speech and sound detection [23]. Considering the problem of separating a single source out of several mixture of sounds, separation of simultaneous and independent sources in indoor scenarios was done in [24]. In [25], the second-order statistics was introduced based on a joint diagonalization of a set of covariance matrices. Regarding the fourth-order statistics, a joint approximate diagonalization of eigenmatrices (JADE) algorithm was introduced by Cardoso and Souloumiac [26], which is one of the most well-known and widely used methods in BSS based on independent component analysis (ICA). It has been shown that linear mixtures can be formulated as generalized eigenvalue decomposition considering the statistical characteristic of sources, such as being non-Gaussian, nonstationary or nonwhite [23]. However, JADE is not optimal in separating heavy-tailed signals such as α -stable processes since such processes usually have no finite second or higher order moments and JADE is based on higher order statistics. Shrimp species create impulsive type noise, which can be modeled through alpha-stable processes [5].

There are studies on more complex mixtures than instantaneous linear ones such as convolutive audio mixtures that consider multipath and delay. In [27], a dynamic frequency-domain algorithm has been proposed for separating audio signals from convolutive sound mixtures. Gur and Niezrecki [28] propose a method to improve the performance of their system regarding BSS. In this method, a known source signal is polluted with ambient noise, but the signal is dominant in comparison with the ambient noise. Godin et al. [29] try to measure the noise level regarding sound-speed measurements with travel time averaging of the signals. Besides these works above, in medical research, finance, and telecommunications, BSS is also applied to analyze the data. A method based on principal component analysis and infinite ICA is developed for feature extraction in [30]. A BSS-based cellular communication solution is proposed in [31] for cloud radio access networks, called Cloud-BSS, which leverages the interbase stations cooperation.

It is worth noting that one of the main challenges in the classification of noise sources is the presence of varying degrees of multipath [32] in the time-varying underwater acoustic channel whose formation is caused by two effects: reflection at the surface, bottom, and by any object and refraction in the water. The latter is caused by the sound-speed variation due to salinity, temperature, and depth, which is mostly evident in deep-water channels. Unknown noise source separation and detection is a challenging problem in this dynamic underwater environment and this is the first study on underwater noise analysis based on BSS.

III. PROBLEM DEFINITION AND PROPOSED SOLUTION

In this section, we consider the problem in detail and organize the proposed solution in the following sections. First, in Section III-A, we address a practical deployment strategy for sensor nodes to form a grid of sensors in the area of study. It is important to structure a defined area in which the proposed

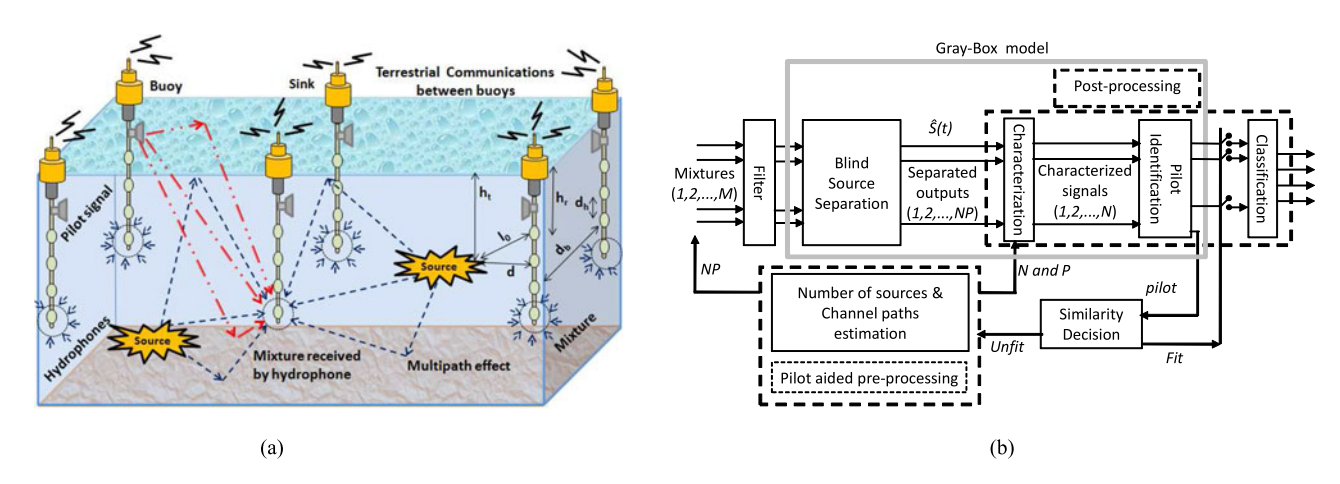


Fig. 4. (a) Proposed deployment of buoys in a multipath underwater environment. Hydrophones are installed on a bar, but buoys are connected to each other via a terrestrial network. (b) Proposed system for UNISeC utilizes the pre- and postprocessing analyses and applies a BSS algorithm in a multipath underwater channel.

method works. We introduce a 3-D ocean environment and a 2-D terrestrial deployment to implement the proposed system. Section III-B explains how our method, called UNISeC, separates and classifies the underwater noise sources. Specifically, our method includes:

- 1) UNISeC, which controls the whole process by estimating unknown parameters of a "gray-box" model;
- 2) underwater noise analysis using BSS.
- 3) a practical instantaneous BSS resulting from a convolutive problem;
- a recursive and least contaminant pilot-aided preprocessing for calculating the number of dominant sources in each frequency subband;
- 5) reliable postprocessing for characterization of the signals using a path-combining technique;
- 6) a pilot-identification procedure and also a classification method to classify the noise sources.

Fig. 4(b) illustrates the block diagram of our proposed method. Finally, in Section III-C, a centralized network structure and some practical aspects are considered.

A. Grid Symmetric Planned Static Deployment

This proposal assumes an architecture in which the hydrophones are anchored to the bottom of the ocean and are connected to the buoys on the surface. The deployment should guarantee a reliable connection between all the network nodes; however, many challenges should be addressed to enable reliable monitoring since:

- 1) hydrophones should actively collaborate in sound capturing to achieve a 3-D coverage of the whole area of interest in the ocean, given their respective sensing ranges;
- 2) hydrophones should be able to relay information to their buoys;
- 3) buoys should be able to connect to the sink station in a wireless 2-D communication.

Considering the cocktail-party problem [24], [31], i.e., separating a single source from a mixture of sounds, different network topologies may lead to different system performance

results. However, in our stated problem, no prior knowledge is available on the power and location of unknown noise sources, which could be used to predict and locate them. Therefore, the best assumption for hydrophone placement would be a uniform distribution, which is appropriate for equiprobable transmitted signals. We call this deployment a symmetric planned arrangement. This refers to the fact that the number of active hydrophones is a measure of noise sources in the environment. Because we consider the case of equal number of mixtures and sources, if one of the hydrophones, for example, is far from one of the sources, the mixtures cannot be separated via the proposed algorithm.

Assume a set $\mathcal{B}=\{B_1,...,B_o\}$ of bottom anchored and fixed buoys with horizontal spacing d_b , with radio transmitters on top, are floating on the surface of the water. Each buoy has m_h omnidirectional hydrophones with a wide frequency range installed on a vertical bar with length $h_r+(m_h-1)d_h$, as depicted in Fig. 4(a), where h_r is the depth of top hydrophone and d_h is the spacing between the other (m_h-1) hydrophones. Therefore, there are in total $M=B_om_h$ hydrophones in an underwater 3-D deployment architecture in addition to the terrestrial 2-D wireless radio network formed by the buoys on the sea surface. Note that surface-level radio channels are assumed to be benign in this paper and we leave the consideration of unreliable radio channels for future work. We consider the following assumptions:

- internal noise of hydrophones is less than dominant ambient noise level in the environment, such as depicted in Fig. 2;
- hydrophones should be robust against the pressure when depth increases;
- 3) thermal noise due to cable connections to the water surface and the buoy is negligible.
- 1) Terrestrial 2-D Grid: Since BSS analysis needs all the data to be collected simultaneously in one node, we assume one of the buoys plays the role of sink to gather the information from B_o-1 remaining buoys in a terrestrial network after it records its own sounds captured by its hydrophones in the

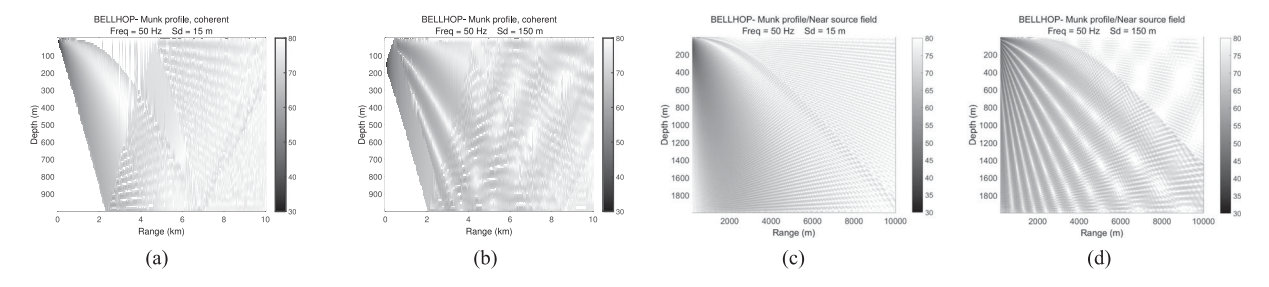


Fig. 5. (a) Transmission loss calculated by Bellhop for a sample source near surface. Source depth is 15 m. (b) When the source is far from surface, for example, source depth is 150 m. (c) and (d) Near-field influence of a sample noise source for different depths, i.e., 15 and 150 m, respectively.

underwater scenario. Clearly, the sink buoy should be powerful enough and should have enough resources to perform the signal separation duties after collecting the recorded data and also to communicate with the buoys to issue appropriate commands and synchronization signals. Furthermore, the distance between the adjacent buoys, i.e., d_b , should provide communication coverage over the area of interest. We will discuss the detail later in Section III-C.

2) Underwater 3-D Deployment: The received signals at hydrophones are influenced by many factors such as channel transmission loss, background noise, multipath effect, Doppler spread, and high and variable propagation delay [2]. Considering temperature, salinity, and pressure of the body of water traversed, sound speed varies between 1450 and 1540 m/s and so small changes in speed lead to significant changes in the sound propagation in the ocean [33]. Furthermore, sound reflection from the surface and bottom and other objects in the ocean and also other minor effects such as sound refraction form a multipath effect propagation, which is the result of spatial variability of sound speed regarding depth and location [34]. The multipath geometry relates to the channel configuration. Vertical channels are specified by little time dispersion, whereas horizontal channels may have extremely long multipath spreads, regarding the water depth [2].

In this paper, we consider the path loss model defined in [35] and [36], i.e.,

$$\mathcal{A}(\ell, f) = \mathcal{A}_0 \ell^k a(f)^\ell \tag{1}$$

where $\mathcal{A}(\ell, f)$ is the experienced path loss (attenuation) on a single path, A_0 is a normalizing constant, ℓ [m] is the distance, f [Hz] is a tone of frequency, k is the spreading factor whose value is normally 2, and a(f) is the absorption coefficient [33, pp. 10–12], as $10 \log a(f) = a'(f) = 0.11f^2/(1+f^2) +$ $44f^2/(4100+f^2)+2.75\times 10^{-4}f^2+0.003$ [35], [36]. In this empirical formula, f is in kilohertz and $10 \log a(f)$ is obtained in decibel per kilometer. a(f) (in per meter) is obtained as $a(f) = 10^{a'(f/1000)/10000}$, where f is in hertz. Note that this definition of path loss does not consider the total power. When considering multiple propagation paths, in which the signal at the receiver is the outcome of several delayed signals of the original signal, the channel transfer function (CTF) of each path p is $H_p(f) = \Gamma_p / \sqrt{\mathcal{A}(\ell_p, f)}$, where Γ_p is the cumulative reflection coefficient containing surface and bottom reflections of each path. The overall CTF with multipath is calculated as $H(f) = \sum_{p} H_p(f) e^{j\theta_p(f)}$, in which $\theta_p(f)$ is the phase response characteristic for the path p. Delay characteristic can be defined as $\tau_p = -1/(2\pi) d\theta_p(f)/df$ and it represents the propagation delay associated with the path p. This delay can be modeled as $\tau_p = \ell_p/c - \ell_0/c$, where c, ℓ_0 , and ℓ_p stand for the sound speed, the first path distance, and the pth path distance, respectively. Fig. 5, using Bellhop acoustic beam tracing model [37], illustrates the effect of transmission loss in the underwater channel for a sample source in different depths as a function of distance. The farther we go from the source, the more we observe a power level decrease. Transmission loss between a standard reference range, i.e., 1 [m], and the distance in which the signal is received is shown in Fig. 5. The transmission loss shown in this figure is calculated over the total paths considering the details of the channel geometry. While this knowledge on the channel is hard to obtain in a real setting, we provided another method for path loss per path in (1). Since we might have more than one source in the area and the locations of noise sources are unknown, UNISeC, discussed in the following section, tries to find the appropriate number of sensors for activation. Hydrophone activation means that they are turned on to collect data. We assume that all the noise sources are in the same region of interest as hydrophones. If ℓ_d is the longest diagonal in the area of interest defined in Fig. 4(a) and we define it as $\ell_d = \sqrt{((B_o/2 - 1)d_b)^2 + {d_b}^2 + {d_z}^2}$, where d_z is the water depth and $d_z > h_r + (m_h - 1)d_h$, then the delay associated with this path is defined as the largest line of sight (LOS) propagation delay, $\tau_{0\max} \approx \ell_d/c$. Therefore, if we have several sources in this area, their LOS delays are less than $\tau_{0 \, \text{max}}$, i.e., $\tau_{n0} \leqslant \tau_{0\text{max}}$, where $\tau_{n0} \quad \forall n = 0, ..., N$ denotes the propagation delay for the nth source. Similar calculations can be done for the path p in a multipath channel.

Let us assume that the received signal-to-noise ratio (SNR) per path, as a function of frequency, distance, and the environmental conditions, is mainly affected by path loss per path defined in (1). For the longest diagonal distance, we have $\mathcal{A}(\ell_d,f) = \mathcal{A}_0(\ell_d)^k a(f)^{\ell_d}$ and the received SNR can be written as [34] $\gamma_r = S_{\ell_d}(f)/(\mathcal{A}(\ell_d,f)N(f))$, where S_{ℓ_d} is the PSD of the transmitted signal, and N(f) is the nondominant background noise PSD. Therefore, ℓ_d should guarantee $\gamma_r > \gamma_{\rm th}$, in which $\gamma_{\rm th}$ stands for the lowest detectable SNR (we considered the SNR per path) in the hydrophone, i.e.,

$$\frac{S_{\ell_d}(f)}{\mathcal{A}_0 c^k \tau^k a(f)^{c\tau} N(f)} > \gamma_{\text{th}}.$$
 (2)

The maximum acceptable delay can be calculated via

$$\tau^k a(f)^{c\tau} < \frac{S_{\ell_d}(f)}{\mathcal{A}_0 c^k N(f) \gamma_{\text{th}}} \tag{3}$$

$$k \ln(\tau) + \tau c \ln a(f) < \ln \left(\frac{\gamma_{\ell_d}}{\mathcal{A}_0 c^k \gamma_{\text{th}}}\right).$$
 (4)

In (4), γ_{ℓ_d} corresponds to a certain source power at distance ℓ_d over the power of background noise in the environment.

$$c\tau \ln a(f) + k \ln \left(\frac{c \ln a(f)}{k}\tau\right) < \ln \left(\frac{\gamma_{\ell_d}}{\mathcal{A}_0 c^k \gamma_{\text{th}}}\right) + k \ln \left(\frac{c \ln a(f)}{k}\right)$$
(5)

$$\frac{c \ln a(f)}{k} \tau \exp\left(\frac{c \ln a(f)}{k} \tau\right) < \frac{c \ln a(f)}{k} \exp\left(\frac{\ln \left(\frac{\gamma_{\ell_d}}{A_0 c^k \gamma_{\text{th}}}\right)}{k}\right). \tag{6}$$

Lambert W() function can be used to find a closed-form expression for the above inequality as follows:

$$\frac{c \ln a(f)}{k} \tau < \mathcal{W}\left(\frac{c \ln a(f)}{k} \exp\left(\frac{\ln\left(\frac{\gamma_{\ell_d}}{\mathcal{A}_0 c^k \gamma_{\text{th}}}\right)}{k}\right)\right) \tag{7}$$

$$\tau < \frac{k}{c \ln a(f)} \mathcal{W} \left(\frac{c \ln a(f)}{k} \left(\frac{\gamma_{\ell_d}}{\mathcal{A}_0 c^k \gamma_{\text{th}}} \right)^{1/k} \right). \quad (8)$$

Let us assume that $\tau_{\rm pm\,ax}$ converts the above inequality to equality and represents the maximum tolerable delay of the system for receiving the reflected signals. Therefore, for all the delays τ_{np} of path p and source n

$$\tau_{np} < \tau_{\text{pmax}} \quad \forall p = 0, ..., P \text{ and } \forall n = 0, ..., N.$$
(9)

As a result, (3) and (9) ensure that the path with the longer length has a longer propagation delay and so it will be ignored if it is slower than $\tau_{\rm pmax}.$ We interpret this method as a temporal filtering that cleans up the undesirable delayed paths in a multipath channel. On the other hand, since there is no information on the noise sources, their transmitted power, i.e., $S_{\ell_d}(f)$, is completely unknown and we have to approximate (3) for a known pilot signal Π as $\tau_p \approx \tau_\Pi$. Later, this information is applied to the Gray-box model to find an appropriate solution for the required parameters.

B. UNISeC: Underwater Noise Inspection, Separation, and Classification System

This section provides information on modeling the proposed system, UNISeC, for separation and classification of any number of underwater noise sources. Let us consider the block diagram in Fig. 4(b) and study every single block in detail as follows: BSS, filtering, pilot-aided preprocessing, gray-box modeling and the algorithm, postprocessing that covers characterization, pilot identification, and classification blocks.

1) Blind Source Separation: In blind identification techniques, all sources, signals, and mixing coefficients are unknown except the observed mixtures. If S(t) represents the matrix of N signals and X(t) is the observation matrix, formed by M

mixtures, a simple mixing model is X(t) = AS(t), in which the observation is a linear combination of input signals and A stands for the mixing matrix. This model is known as instantaneous mixture. Under the assumption that ICA is used for separation, input signals should be independent, i.e., $E\left\{S(t)S(t)^H\right\}$ is diagonal, and H denotes the Hermitian transpose. This assumption, e.g., independence of the sources, is realistic and illustrated by means of examples in Fig. 2 since independent sources emit statistically independent signals. Fig. 3 presents various examples confirming non-Gaussianity of noise sources that makes this problem appropriate for ICA-based BSS.

Our goal is to form a separating matrix \hat{A} to apply to the mixtures so the matrix of sources' signals can be estimated as $Y(t) = \hat{A}X(t)$. However, in many physical applications, the mixtures correspond to the sum of the multiple weighted and delayed signals. This kind of mixing model is known as convolutive mixture. In this section, we deal with converting the convolutive problem to an instantaneous BSS since its complexity is less and its accuracy is higher than the convolutive problem. The received signal at each hydrophone is a mixture of all noise signals coming from a multipath channel. We aim at separating the signals via BSS [38], characterizing main signals, and classifying them into known underwater noise categories. If $s_n(t)$ represents a dominant noise source n, n = 1, ..., Nwhich is generally non-Gaussian, colored, and statistically independent of the other sources, then $x^{m}(t)$ is the received signal at hydrophone m, m = 1, ..., M and can be formulated as a convolutive mixture at time t as follows:

$$x^{m}(t) = \sum_{n=1}^{N} \sum_{p=1}^{P} a_{np}^{m}(t) s_{n}(t - \tau_{np}) + z^{m}(t)$$
 (10)

where $a_{np}^m(t)$ is the mixing coefficient of the pth path between the nth source and the mth sensor as the receiver with corresponding delay τ_{np} and $z^m(t)$ stands for the nondominant background noise which can be assumed as additive white Gaussian noise. Note that in this approach, we cannot employ absolute path delays. However, in practice, we do not require to calculate the absolute values since our method measures the similarity between the separated outputs in postprocessing computation for characterization, pilot identification, and classification.

In this approach, the assumption of independent paths is valid if the paths are well separated. We define the paths to be separated when the signals received from different paths are not overlapped in all domains. If the paths are not well separated, the output of the BSS would be the mixture of the nonseparated paths. In practical situations, if there is any correlation between the paths, a mixed output is observed which looks like some fading has occurred. On the other hand, since we perform postprocessing to characterize the main path among the separated outputs, it is not really a problem. Moreover, it is shown in [38] that if the delay between the correlated paths is greater than the symbol duration (which is the case in underwater), JADE can still separate these correlated paths. In other words, an underwater channel response is said to be a sparse and a convolutive problem that can be seen as an instantaneous one as follows.

We define $\tilde{s}_{np}(t) = s_n(t - \tau_{np})$, $\tilde{a}_n^m = [a_{n1}^m \ a_{n2}^m \dots a_{np}^m]$, and also $\tilde{s}_n = [\tilde{s}_{n1} \ \tilde{s}_{n2} \dots \tilde{s}_{np}]$ in which we eliminated "t" for simplicity. We rewrite (10) as

$$x^{m}(t) = \begin{bmatrix} \tilde{a}_{1}^{m} \ \tilde{a}_{2}^{m} \ \dots \ \tilde{a}_{N}^{m} \end{bmatrix} \begin{bmatrix} \tilde{s}_{1}^{T} \ \tilde{s}_{2}^{T} \ \dots \ \tilde{s}_{N}^{T} \end{bmatrix}^{T} + z^{m}(t) \quad (11)$$

where T denotes the transpose.

Let us now define

$$\tilde{A}(t) = \begin{bmatrix} \tilde{a}_{1}^{1} & \tilde{a}_{2}^{1} & \dots & \tilde{a}_{N}^{1} \\ \vdots & \vdots & \vdots & \vdots \\ \tilde{a}_{1}^{M} & \tilde{a}_{2}^{M} & \dots & \tilde{a}_{N}^{M} \end{bmatrix}$$
(12)

and $\tilde{S}(t) = [\tilde{s}_1^T \ \tilde{s}_2^T \ \dots \ \tilde{s}_N^T]^T$, X(t) is the $M \times 1$ vector containing all the mixtures at t, which can be written as

$$X(t) = \tilde{A}(t)\tilde{S}(t) + Z(t). \tag{13}$$

The equation now contains instantaneous mixtures and can be solved via an instantaneous BSS algorithm. Note that for applying BSS, the number of sources and paths in the channel should be determined, and the number of hydrophones should be equal to or greater than the product of sources and paths, i.e., $M \geq NP$. The number of sources are limited in practice and we can assume that they are less than hydrophones; therefore, we consider the case of well-determined BSS in this section. It is worth noting that since BSS generally addresses the statistical independence using higher order statistics, and due to the situation we face in the underwater environment, i.e., generally non-Gaussian sources, we use algorithms based on the fourth-order statistics in our calculations.

First, let us start with the concept of source mutual independence and second-order statistics, i.e., covariance matrix, as $\hat{R}_{\tilde{s}} = E\{\tilde{S}(t)\tilde{S}^H(t)\}$ which is diagonal and so $\hat{R}_x =$ $E\{X(t)X^H(t)\}$, where \hat{R}_x is the covariance matrix of the mixtures and $R_{\tilde{s}}$ stands for the covariance matrix of independent noise sources. Considering a robust algorithm such as JADE [26], which is an ICA-based blind beamformer for estimating the unknown parameters, we can calculate a whitening matrix \hat{W} . Let μ_1, \ldots, μ_{NP} be the NP largest eigenvalues and h_1, \ldots, h_{NP} be the corresponding eigenvectors of \hat{R}_x ; hence, whitener matrix can be achieved by eigendecomposition of \hat{R}_x via $\hat{W} = [(\mu_1 - \hat{\sigma})^{-\frac{1}{2}} h_1, ..., (\mu_{NP} - \hat{\sigma})^{-\frac{1}{2}} h_{NP}]^H$ where $\hat{\sigma}$ is the variance of nondominant background noise Z, which can assumed to be white. The most important issue in this step is how to estimate NP. UNISeC will try to address this problem in the following section.

Second, we form the fourth-order cumulants of the whitened process $\hat{B}(t)$. This process is the result of multiplying the whitening matrix by mixture matrix as $\hat{B}(t) = \hat{W}X(t) = \hat{W}(\tilde{A}(t)\hat{S}(t) + Z(t))$ exploited to find NP most significant eigenpairs $\{\hat{\lambda_r}, \hat{M_r} \mid 1 \leqslant r \leqslant NP\}$, where $\hat{\lambda_r}$ s are real eigenvalues and $\hat{M_r}$ s are eigenmatrices obtained from the fourth-order cumulants of our complex random vector. Fourth-order cumulants are defined as $\Gamma_{\hat{B}} = \operatorname{Cum}(\hat{b}_i, \hat{b}_j^*, \hat{b}_k, \hat{b}_l^*)$ where $1 \leqslant i, j, k, l \leqslant NP$ and so $\Gamma_{\hat{B}} = E(\hat{b}_i\hat{b}_j^*\hat{b}_k\hat{b}_l^*) - E(\hat{b}_i\hat{b}_j^*)E(\hat{b}_k\hat{b}_l^*) - E(\hat{b}_i\hat{b}_j^*)E(\hat{b}_k\hat{b}_l^*)$, whereas \hat{b}_i s are arbitrary

columns of matrix \hat{B} . Cumulant matrices were introduced by Cardoso and Souloumiac [26] and denoted by $Q_{\hat{B}}(\hat{M}_r)$ with any $NP \times NP$ matrix \hat{M}_r and a Hermitian matrix $Q = (q_{ij})$ and are defined as $q_{ij} = \sum_{k,l=1,\dots,NP} \operatorname{Cum}(\hat{b}_i,\hat{b}_j^*,\hat{b}_k,\hat{b}_l^*)m_{lk},$ where $1 \leqslant i,j \leqslant NP$ and m_{lk} s are the entries of matrix \hat{M}_r . Based on the proposition presented by Cardoso and Souloumiac [26], for any NP-dimensional complex random vector v with fourth-order cumulants, there exist $(NP)^2$ real eigenvalues $\lambda_1,\dots,\lambda_{(NP)^2}$ and $(NP)^2$ eigen matrices $M_1,\dots,M_{(NP)^2}$ satisfying $Q_v(M_r) = \lambda_r M_r, 1 \leqslant r \leqslant (NP)^2$. However, the reduced set of NP matrices, instead of $(NP)^2$, contains the relevant fourth-order information.

In the third step, the cumulant matrix is diagonalized by a unitary matrix \hat{U} formed by $Q_B(\hat{M}_r) = \hat{U}\Lambda_{\hat{M}_r}\hat{U}^H$ [26]. Hence, we jointly diagonalize the set $\{\hat{\lambda}_r\hat{M}_r \mid 1\leqslant r\leqslant NP\}$ by \hat{U} . Joint diagonalization can be implemented via standard Jacobi algorithm [39]. Finally, after determining \hat{U} , we can estimate \hat{A} as $\hat{A} = \hat{W}^\#\hat{U}$ and use this value to extract the sources out of the mixtures in BSS block in the algorithm. $\hat{W}^\#$ is the pseudoinverse of \hat{W} and can be computed easily via $\hat{W}^\# = [(\mu_1 - \hat{\sigma})^{\frac{1}{2}}h_1, \ldots, (\mu_{NP} - \hat{\sigma})^{\frac{1}{2}}h_{NP}]$. Considering Fig. 4(b), other components of UNISeC are as follows.

- 2) Filtering and Pilot-Aided Preprocessing: In this section, preprocessing, filtering, dominant noise definition, and features of pilot will be discussed.
- a) Tunable and band-limited filter with variable central frequency: As previously explained, our goal is to investigate the dominant noise sources in desired subbands. The analysis, based on the common octave band and one-third octave band filters [9], implies that the filter bandwidth is proportional to its central frequency. This ratio is 70.7% and 23% of the center frequency in a 1-octave band and a 1/3-octave filter, respectively. Thus, for center frequency f_c , a 1-octave band is from $(2^{-\frac{1}{2}})f_c$ to $(2^{\frac{1}{2}})f_c$ or from $0.707f_c$ to $1.414f_c$. Similarly, it is from $(2^{-\frac{1}{6}})f_c$ to $(2^{\frac{1}{6}})f_c$ or from $0.891f_c$ to $1.122f_c$ for a 1/3-octave band. Since in humans and some animals, the effective filter bandwidth of the hearing system is 1/3-octave, in practice, 1/3-octave band is more frequently used to present the behavioral thresholds [9]. Behavioral thresholds of sound are levels in which animals react with some psychological/behavioral responses. Inspired by this fact, we first divide the frequency bands into nonoverlapping subbands via a series of narrow bandpass filters. Subsequently, we perform UNISeC on each subband separately. Bandwidth of filters are variable and calculated regarding the available information on spectral characteristics of underwater noise signals as reported in [8] and [9]. Moreover, it is desirable to perform the filtering such that limited number of dominant sources are available in each subband and the leakage from other subbands is prevented, so the transition width of the filter should be small. Passband and stopband ripples do not play any critical role in our problem and so the minimum order finite-impulse response design is applicable since it is stable inherently and it can be considered as a linear-phase filter.
- b) Dominant noise definition: Spectral analysis of common noise sources reveals that acoustic noise generated from

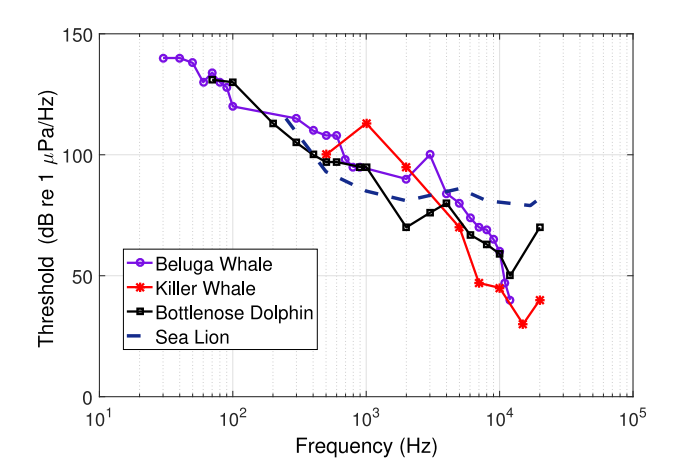


Fig. 6. Behavioral audiogram for several marine species versus frequency. Any sound is detectable only if the received level of the sound exceeds a certain detection threshold. In this figure, marine mammal nominal reaction/response level is depicted versus frequency to figure out their abilities to detect and respond to man-made sounds. Data were obtained from [9].

seismic, shipping, drilling, and sonar activities spans over a wide range of frequencies and varies with location, depth, season, and time of the day; however, each of these sources is dominant in a specific band in the area of interest. By dominant we mean a signal which is stronger than the regular background noise and so it might be audible by the mammals. This threshold also varies with the environment and depends on the hearing abilities of mammals. As an example of dominant noise, seismic noise is dominant in the extremely low frequency band, i.e., below 1 Hz, while ocean turbulence is dominant in the very low frequency band, i.e., from 1 to 10 Hz. Vessels are the main contributors of the noise and several types of them dominate from 10 to midhundreds hertz. Ships are significant in deep ocean and starting from 10 Hz, while fishing boats are dominant in coastal regions and start from 200 Hz. Above 300 Hz, shipping noise may or may not be significant depending on the level of wave and wind noise [9]. Wave and wind noise are dominant from midhundreds hertz to 50 kHz [8]; also, thermal noise is dominant after 50 kHz; and the sound by marine mammals such as whales is dominant from 30 Hz to 10 kHz [9].

c) Required features for least contaminant pilot-aided probing: According to UNISeC algorithm, the pilot sequence is propagated and received along with the other noise signals. This signal should be weaker than the response threshold level of marine mammals to prevent any behavioral reactions. On the other hand, it should be stronger than the regular background noise, so the background noise does not affect the detection of the pilot signal by regular sensitivity hydrophones installed in different locations. $\gamma_{\rm II}$ equals pilot power in subband Δ to background noise power in the same subband, and satisfies the following inequality:

$$(\gamma_{\text{th}})_{\Delta}[dB] < 10 \log_{10} \left(\frac{\int_{f_1}^{f_2} S_{\Pi}(f) df}{\int_{f_1}^{f_2} G_z(f) df} \right) < \rho_{\Delta}[dB]$$
 (14)

whereas $(\gamma_{\rm th})_{\Delta}$ stands for the lowest detectable input SNR in the hydrophone or in other words its sensitivity, f_1 and f_2 are lower

and upper frequencies of each subband Δ , $S_{\Pi}(f)$ and $G_z(f)$ are pilot signal and background noise PSD, respectively, and ρ_{Δ} shows the nominal response threshold level of mammals in each subband. Regarding data provided in [9], behavioral reactions and sensitivities of marine mammals to sound are different and are shown by audiograms in Fig. 6 for some species. All the mentioned species can hear the sound within a wide range of frequencies; however, the results vary from one species to another. These data [9] were gathered by electrophysiological tests on trained captive or beached animals. According to studies in [9], the behavioral method presents pure tones at various levels and frequencies to a trained animal. The audiogram data can be used to set the pilot signal level thresholds.

3) Gray-Box Model, Iterative Algorithm for UNISeC: The described algorithm uses MCC to extract the pilot signal and other main signals. The similarity between the estimated pilot and the original one is calculated via MSCE metric Ψ to find the value of NP. To initialize Algorithm 1, let us assume a minimum value for number of paths as P_0 , as a priori knowledge, and a minimum value for the number of dominant sources as N_0 and $M_{0}^{'}=N_{0}P_{0}$. $M_{0}^{'}$ would be remembered as the minimum required number of active sensors. To select these initialization values, we consider the theoretical channel model of the environment of the study and the minimum number of the dominant noise sources in the desired subband for the available physical information as of Fig. 2. As explained in the first line of Algorithm 1, initialization is performed; then in line 2, the desired subband is chosen. For a specific bandwidth Δ , the initial location of pilot is determined and the iteration index κ is initiated. In phase I, started from line 5, pilot is circulated in all the buoys, BSS-JADE is called, and the pilot signal among all the other separated outputs is characterized and identified (lines 7 and 8). If the corresponding similarity threshold is satisfied (lines 9 and 10), the value of binary fitting index ϖ is assigned to 1 (line 11). ϖ allows us to understand the correctness of Gray-box model proposed in (17c). Phase II, started from line 16, makes the final decision based on total ϖ , i.e., ϖ_T . This value collects local ϖ s, weights them regarding the similarity values, and compares them with the similarity threshold Th_{Ψ} defined as follows:

$$\varpi_T = \frac{1}{B_o} \sum_{b=1}^{B_o} \Psi_b \varpi_b \tag{15a}$$

$$Th_{\Psi} = \xi(1 - Th_{\mathrm{Err}}). \tag{15b}$$

This metric fulfills the model fitting with confidence degree of $\xi\%$. Let ξ be 50%, which means at least half of fitting indices pass the fitting test. When the fitting conditions are not satisfied, the number of mixtures has been underestimated. Thus, we increase the iteration κ in step 21. The algorithm runs with a larger number of active sensors, which is calculated stepwise as follows, for the κ th iteration:

$$M_{\kappa}^{'} = M_{0}^{'} + \kappa \min(P_{0}, N_{0}).$$
 (16)

Note that $\min(P_0, N_0)$ can be assumed I when there is no information on the channel or can be more than 1, due to the channel model knowledge, to accelerate the convergence of the algorithm. If the number of current active sensors is greater

Algorithm 1: Set of rules for the UNISeC.

```
Input: X(t), M, B_o, N_0 P_0,
Output: [M'_{\kappa}]_{\Delta} = NP and [S_{CL}(t)]_{\Delta};
  1: Start: Initialize [M_0']_0 \leftarrow N_0 P_0 \triangleright activate initial sensors
 2: for all subbands \Delta = 0 : BW, do \{ \triangleright \text{ narrow the band} \}
 3:
         repeat
          \kappa \leftarrow 0, b \leftarrow \text{random selection}([1, B_o]) > initialization
 4:
 5:
           Phase I: Separation and Pilot location
           circulation
 6:
           for b; 1 : B_o, do
 7:
             Calculate [M'_{\kappa}]_{\Delta} as (16); Call
             BSS-JADE([M'_{\kappa}]_{\Delta})
 8:
             Call MCC for (\hat{S}(t)); Call MSCE for (\hat{S}_{\square}(t), \Pi)
 9:
             Find the similarity \Psi_b and \Psi_{bErr} for \Pi
10:
             if \Psi_{bErr} < Th_{Err} AND \Psi_{bD} > Th_D then
11:
                \varpi_b \leftarrow 1 \triangleright binary fitting index (\varpi) after
               (17d), (17e)
12:
             else
13:
                \varpi_b \leftarrow 0
             end if
14:
15:
           end for
16:
           Phase II: Fitting decision
17:
           Find \varpi_T as in (15a)
                                                     \triangleright Total fitting index
18:
           if \varpi_T > Th_{\Psi} then \{ \rhd Th_{\Psi} \text{ is similarity threshold} \}
19:
             Goto Phase III
                                       ⊳ when passes fitting decision
20:
             \kappa \leftarrow \kappa + 1; Update [M'_{\kappa}]_{\Delta} as (16)
21:
22:
             if M_{\kappa}^{'} > M then
23:
                Reduce \Delta to cut the number of dominant
             sources; goto step 4
24:
             else
25:
                Activate a new sensor and goto Phase I
26:
               \triangleright Estimator model \mathcal{G} is unfit in (17b) and (17c)
27:
             end if
28:
           end if
29:
         until [M_{\kappa}^{'}]_{\Delta} is fit
         return [M'_{\kappa}]_{\Delta} = NP
30:
         Phase III: classification, call MSCE function
31:
32:
         return [S_{CL}(t)]_{\Delta}
                                                  \triangleright Classified signal
33: end for
34: while \Psi_{Err} < Th_{Err} do
35:
         Turn off pilot
         Redo steps 7–9 for [M'_{\kappa-1}]_{\Lambda=0\cdot BW} > separation \ w/o
36:
         pilot
37: end while
38: Goto step 1
```

than the total available ones, UNISeC reduces the bandwidth to cut the number of dominant sources and starts the procedure over from step 4. Otherwise, new sensors are activated and algorithm goes back to phase I for pilot circulation with the updated number of sensors, reflected in steps 22–27. Scaling and permutation ambiguity [38] that might happen in BSS will be alleviated when we repeat the similar test from different buoys. Phase III classifies the separated signals. Lines 34–37 stand for steady-state period of UNISeC in which the separation

proceeds without involving pilot signal until a significant change is observed in similar values. Transient and steady-state periods will be discussed in Section III-C.

As shown in Fig. 4(b), the main part of the proposed model is defined as a *Gray-box* block. To explain the motivation behind this definition, we should notice that although the mathematical model for BSS is reliable, some validations and knowledge are needed to complete the theoretical model and estimate the unknown parameters. Inspired by the concept of Gray-box modeling [40], we define a novel model that contains BSS and its subsequent processing as a class of parametric model which needs to be fit with some parameter tuning according to some experiments. The parameter estimation includes finding the filter bandwidth, number of required sensors, and the acceptable amount of similarity for the pilot. This Gray-box model tries to optimize the process by minimizing the deviation between measured data and the response of the model and distinguishes it from conventional black- or white-box modeling. We call it the Gray-box model to emphasize on its hybrid nature, which is neither a black-box nor a white-box approach. Let us define the Gray-box model \mathscr{G} and its estimator \mathscr{G} as

$$Model: \mathcal{G}\{X(t), \Psi, M\} \to \{S(t)|M\}$$
 (17a)

Estimator:
$$\bar{\mathscr{G}}\left\{\tilde{X}(t), \Psi_{\Pi}, [M_{\kappa}', T, f_s, B^{\Pi}]_{\Delta}\right\}$$
 (17b)

$$\rightarrow \left\{\hat{S}(t), \hat{S}_{\square}(t) \middle| [M_{\kappa}', T, f_s, B^{\Pi}]_{\Delta}\right\}$$

$$\text{Fitting}: \text{min}_{\kappa} \bar{\mathscr{L}} \Big\{ \Psi_D, \Psi_{\text{Err}} \Big(\Pi, \big\{ \hat{S}(t), \hat{S}_{\square}(t) \big|$$

$$[M'_{\kappa}, T, f_s, B^{\Pi}]_{\Delta}\}$$
 (17c)

Error Test :
$$\Psi_{\rm Err} < Th_{\rm Err}$$
 (17d)

Reliability Test:
$$\Psi_D > Th_D$$
 (17e)

where X(t) and X(t) reflect the mixtures as the input sequence in the model \mathscr{G} and the practical estimator $\overline{\mathscr{G}}$ in subband Δ ; Mand M_{κ}' are defined by (16) and determine the variable parameters for the minimum required number of active sensors; Π and B^{Π} are used for pilot signal and its current location on buoy B; T stands for the recording interval; f_s is the sampling frequency; S(t) represents the original output of separation in the model; and $\hat{S}(t)$ and $\hat{S}_{\vdash}(t)$ denote the output of separation and identification process in the estimator, respectively. Regarding the parameter M or M'_{κ} , the model or estimator aims to minimize the given average loss function $\bar{\mathscr{L}}$ subject to the parameter setting to keep $\Psi_{\rm Err}$ under a specific threshold, i.e., $Th_{\rm Err}$, defined in (22), by changing the parameters to fit the pilot with the main separated output. Ψ_D is defined as the relative distance and will be quantified in (22b). This metric is a measure of reliability compared with a threshold Th_D .

The main difference between the model and the estimator originates from different facts; the estimator uses both prior knowledge and new parameters as the response from experiments on the pilot. Prior knowledge must be able to convert the primary model $\mathscr G$ into the algorithm simply so that simulation can be performed, the derivation of the estimator $\mathscr G$ is practical, and finally fitting the parameters can be satisfied. Output of the

fitting test determines if the procedure should continue or it is the appropriate time to stop. The process will be repeated until convergence satisfies. This is the technique we use to solve the minimization procedure in the proposed model in (17), since we aim to find the value of the parameters, i.e., number of unknown sources. Note that the proposed model will be stable if the validation procedure leads to an MSCE which satisfies the fitting test.

4) Postprocessing: It contains the following components.

a) Characterization and pilot identification: Outputs of BSS block are associated with NP paths; each group of P signals belongs to one of the N sources. Among these signals, we just require the N main ones; thus, we propose a selection combining approach to characterize them among NP separated outputs. MCC is exploited for selection combining among every P outputs to provide an estimate of the correlation between the sampled sequences $\hat{S}_i(t)$ and $\hat{S}_j(t)$ for $i,j=1,2,\ldots,NP$ as

$$R_{ij}[m] = E\left\{\hat{S}_i[n+m]\hat{S}_j^*[n]\right\}$$
 (18)

where m and n stand for discrete time index, asterisk represents complex conjugation, and $E\{.\}$ denotes the expectation operator. Regarding the theory behind (18), E requires the probability distribution function of the noise (which is unknown), while for $-\infty < n < \infty$ this computation is not practical. In practice, since only a finite segment of length N_S is available, we have to use an estimation of correlation as

$$\hat{R}_{ij}(m) = \begin{cases} \sum_{n=0}^{N_S - m - 1} \hat{S}_i[n+m] \hat{S}_j^*[n], & m \ge 0\\ \hat{R}_{ii}^*(-m) & m < 0. \end{cases}$$
(19)

We perform normalization to produce a comparable estimate for correlation. By definition, the normalized cross correlation $||\hat{R}_{ij}(m)||$ relates to $\hat{R}_{ij}(m)$ via

$$||\hat{R}_{ij}(m)|| = \frac{\hat{R}_{ij}(m)}{\sqrt{\hat{R}_{ii}(0)\hat{R}_{jj}(0)}}.$$
 (20)

Instead of clustering the outputs to extract the main signals, MCC expedites this process and characterizes the main signals as its output, in one step, so it is definitely much faster than alternative methods. Following the output of characterization, we perform pilot identification, to identify the pilot signal among N main signals. We exploit MSCE metric Ψ , which estimates the coherence of PSD of two output signals. Coherence is computed via MSCE using the Welch's averaged modified periodogram method [41]. MSCE is a function of frequency with values ranging in [0,1] and indicates the similarity of two signals when one of the two signals is known. Output signal having the largest MSCE with the pilot would be labeled as pilot. Coherence is associated with PSD of its inputs as well as of the cross PSD of the two

$$C_{ij}(f) = \frac{|P_{ij}(f)|^2}{|P_{ii}(f)| |P_{jj}(f)|}$$
(21)

in which $P_{ij}(f)$ is the cross PSD of $\hat{S}_i(t)$ and $\hat{S}_j(t)$ and $0 \le C_{ij}(f) \le 1$ for all frequencies. We averaged over frequency to determine the similarity between the two signals.

We use relative distance reliability metric Ψ_D as the difference between the two greatest MSCE values. Considering the

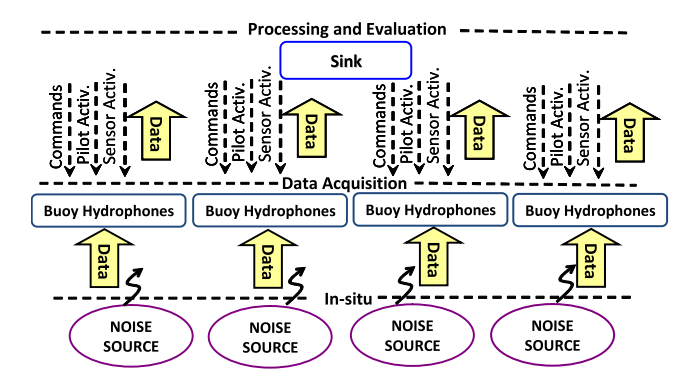


Fig. 7. Proposed centralized structure for UNISeC.

fact that BSS exploits estimation to separate the signals and because many unseen factors in underwater environment might affect it, reliability test checks whether the maximum MSCE is far superior to the second largest one. These metrics are calculated as follows:

$$\Psi_{srt} = \{ \psi_i \mid \psi_i \in \Psi, \psi_i > \psi_{i+1}, \quad i = 1, ..., N \}$$
 (22a)

$$\Psi_D = \frac{\psi_1 - \psi_2}{\psi_1}; \qquad \psi_1, \psi_2 \in \Psi_{srt}$$
 (22b)

$$\Psi_{\rm Err} = 1 - \psi_1; \qquad \psi_1, \in \Psi_{srt} \tag{22c}$$

where Ψ_{srt} is the sorted vector of MSCE in the descending order and Ψ_{Err} was introduced in the loss function $\bar{\mathscr{L}}$ in (17c).

b) Classification: This step is the final goal of this research and allocates signals to the predefined libraries of underwater noise. For this purpose, we exclude the pilot signal among the others after pilot identification and classify the remaining N-1 outputs into the dominant underwater known noise sources, by calculating MSCE between their PSDs. As previously mentioned, MSCE is an appropriate measure of similarity when one of the two signals is given.

Studies on the social behavior of underwater creatures such as dolphins reveal that they live and travel in groups ranging from two to tens of dolphins. They move close to each other as Bottlenose dolphins show some gentle contacts while swimming [42]. In this case and when they are far from the recording hydrophones, they can be approximated as a point source, and it is possible to define a class of sounds under each group to include a school of similar sound sources. Otherwise, when they are not in the same geographic region or they are not close to each other compared to the distance of measurement, they are excluded from our analysis.

C. Centralized Network Structure—Some Practical Aspects

Considering practical implementation, we introduce and envision a centralized structure to study the behavior of UNISeC and its layers interaction. Various events and their corresponding commands are depicted in Fig. 7. The centralized assumption is derived from this fact that UNISeC, along with BSS, manages the whole processing in one node as an onshore and/or a surface sink, since before aggregation of all the recorded signals, separation and processing are not possible. This central node is the one that gives the permission to initiate/terminate the

communication, logs the errors, generates the report, and sends the data to the administrator via a reliable terrestrial connection, as discussed in Section III-A. Report logging is an important task since date of the experiment and the seasonal variations might affect the output of UNISeC. We divide the process into two parts: initialization and transient period, and steady-state period. In initialization and transient period, after buoys are arranged as in Section III-A, preprocessing is implemented for determining the number of dominant noise sources. The recursive process in Algorithm 1 and the Gray-box model are responsible for the quality of outputs as explained in Section III-B. Different types of signals are exchanged between the buoys and the central point, as depicted in Fig. 7. Data signals are the recorded sounds by hydrophones. Control signals include pilot activation/deactivation, sensor activation/deactivation, and other commands. Pilot activation determines the node which should transmit the pilot signal and should consider circulation of pilot location. We circulate the location of pilot sequentially until we get the desired result, as discussed in Algorithm 1. We use relative distance metric Ψ_D , which is a measure of reliability of the pilot circulation under specific distributions of noise sources. Hydrophone activation/deactivation command tries new number of hydrophones on each buoy regarding (16) until fitting test (17c) is satisfied. Other commands such as synchronization is necessary for simultaneous sound capturing. Recording period will be started after the command determines the location of the pilot and active sensors.

It is essential to recognize the following three different time variables.

- 1) Continuous time t, which shows the physical time. This is the time used in the system equations and simulation results, except the last one (see Fig. 18).
- 2) Continuous time T that determines the recording interval and will be discussed in Fig. 18. This parameter can be modified by the user. Longer recording interval means more sampled data which, as a result, can increase the probability of similarity in the fitting test. Furthermore, the startup time of each recording interval is also an important issue since synchronization is a mandatory requirement for BSS.
- 3) Discrete time T which sums up the whole execution time including several recording intervals, pilot circulation, and transmission and processing periods in different subbands of bandwidth BW, i.e.,

$$\bar{\mathbb{T}} \approx \sum_{\Delta}^{\text{BW}} \left[\underbrace{\sum_{\zeta} (T + \check{t}_{\zeta})}_{\text{transient time}} + \underbrace{(T_{CL} + T + \check{t})}_{\text{steady state time}} + (T_{\epsilon}) \right]_{\Delta}$$

where ζ is a function of κ and pilot circulation B^Π and is defined as the number of iterations that the system completes to reach the number of required sensors. The computation might slow down when the number of sources increases, obviously. \check{t} is the processing time, which is a function of the sensor activation/pilot relocation process, and T_{CL} illustrates the required time for the classification process. It is worth noting that \check{t} depends on the number of floating point operations (flops) per clock cycle

TABLE I SIMULATION ASSUMPTIONS: ℓ_{0b} [km] Is the Distance From Source to Buoy B_b , (Π) Is the Pilot Signal, and Loc Shows the Current Location of the Pilot Transmitter

Source	Scenario	Scenario	Scenario	Scenario	Scenario	Scenario
	A	B	C Loc. I	C Loc. II	C Loc. III	C Loc. IV
	$\ell_{01}, \ell_{02} \\ \ell_{03}, \ell_{04}$	$\begin{array}{c} \ell_{01}, \ell_{02} \\ \ell_{03}, \ell_{04} \end{array}$	$\ell_{01}, \ell_{02} \\ \ell_{03}, \ell_{04}$			
1	02, 11	02, 11	02, 11	02, 11	02, 11	2, 11
	05, –	05, –	15, 10	15, 10	15, 10	15, 10
2	12, 03	12, 03	12, 03	12, 03	12, 03	12, 03
	12, -	12, -	12, 09	12, 09	12, 09	12, 09
3	-, -	-,-	15, 12	15, 12	15, 12	15, 12
	-, -	-,-	02, 11	02, 11	02, 11	02, 11
(Π)	06, 06	06, 06	06, 06	12, 12	.01, 12	12, .01
	06, –	06, –	06, 06	12, 12	12, .01	12, 12

handled by the microprocessor. T_{ϵ} represents the time due to system delays.

In the steady-state period, a collision avoidance method is required for coordination among the buoys. Moreover, since we define UNISeC in a well-determined situation, *sleep mode* is defined as the default mode of buoys until the activation command is received from the central point. While the system is working under the determined constraints, explained in the initialization period, the pilot signal is switched off and the output of postprocessing unit is monitored continuously so that whenever system inputs change, UNISeC is prepared to update the values for new constraints, as explained in Algorithm 1 (lines 34–36). We evaluate the computational complexity of the system to make sure that it can work under different circumstances. Inspired by Naik and Wang [43], we compute it in terms of number of real-valued floating point operations (NFP) as

$$\bar{N}_{FP} = 8M^5 + 2\dot{d}(N^2P^2 + M^2) + I(2M^4 + 10M^3 + 30M^2)$$
(24)

where \dot{d} is the number of data samples, M is the number of active sensors, NP is the number of signals to be separated, and I is the iterations for convergence in BSS algorithm in the steady-state period.

IV. PERFORMANCE EVALUATION AND SOUND ANALYSIS

In this section, we discuss the performance results of the presented approach in Section III. The data were extracted from *in situ* measurements of [8, pp. 132–137] and [9]. The channel path loss model defined in [35] and [36] was applied to them to create the input mixtures. Spreading factor in (1) is assumed k=2 and the channel is considered uncorrelated and stationary since it is constant during the processing period. The channel is assumed to be naturally sparse and the number of noise sources in the area of study is limited. We suppose that noise sources are randomly deployed in the environment. Initial sampling rate is 21 kHz and the maximum depth of the water is assumed to be 1000 m. Hydrophones are placed near surface on a bar connected to the buoy with the maximum depth of 20 m and the distance between any two adjacent hydrophones on the same bar is 4 m. Direct distances to the hydrophones are chosen according

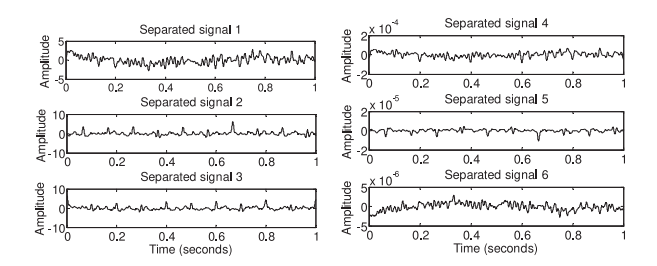


Fig. 8. Output of separation for three signals in a two-path environment in Scenario A.

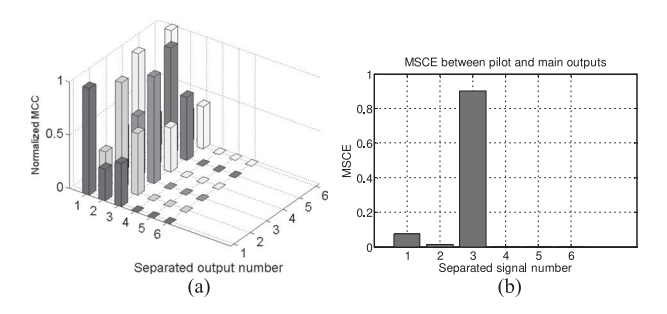


Fig. 9. (a) Output of characterization, normalized MCC between every pair of separated outputs in Scenario A. Signals 1, 2, and 3 are associated with the main paths. (b) Output of pilot identification, i.e., MSCE between pilot signal and main outputs in Scenario A.

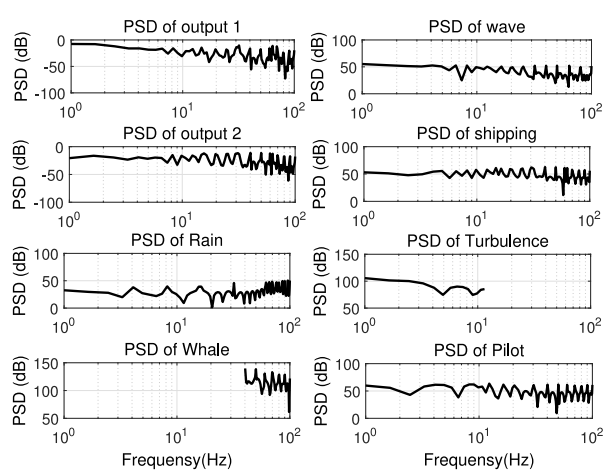


Fig. 10. PSD of the outputs in Scenario A. Filtered spectrum of different classes of noise sources such as wave, shipping, rain, turbulence, and whale noise are shown in this figure.

to Table I. UNISeC is evaluated and simulated under several scenarios. Scenario A checks its validity in the basic mode, i.e., it assumes there are two dominant noise sources located randomly in a two-path environment. Scenario B investigates the effect of multipath by assuming two dominant noise sources in a three-path environment. In Scenario C, we consider the effect of noise traffic and distribution with three noise sources in a three-path channel. Different distributions of noise sources are investigated for all scenarios. Moreover, computational complexity of the algorithm is calculated in several system settings.

A. Scenario A: Basic Mode

In this scenario, we assume two dominant sources in addition to pilot exist in a two-path channel. Fig. 8 shows the output of BSS when six active hydrophones record the mixtures.

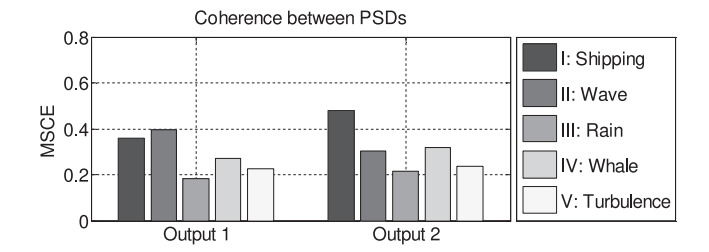


Fig. 11. Classification, i.e., coherency between outputs' PSDs and noise classes in Scenario A. Wave noise and shipping noise are the present sources of noise in the environment.

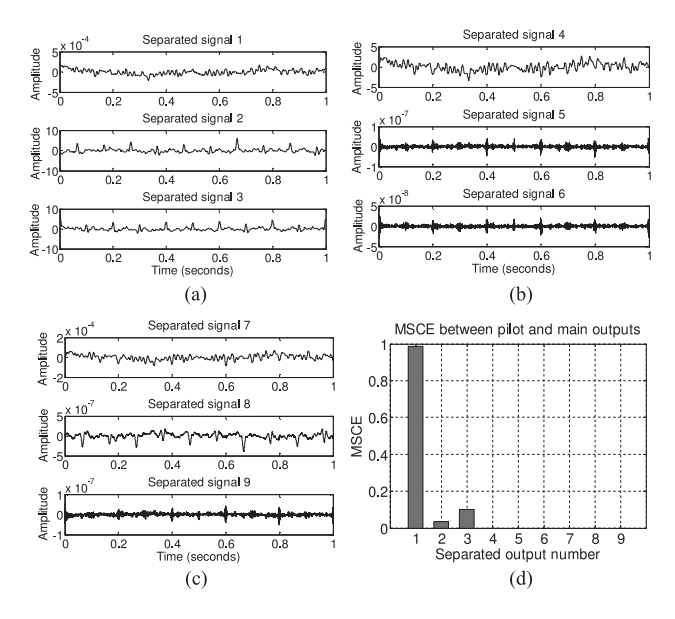


Fig. 12. (a)–(c) Outputs of separation for three sources, in a three-path channel in Scenario B; (d) pilot identification for Scenario B.

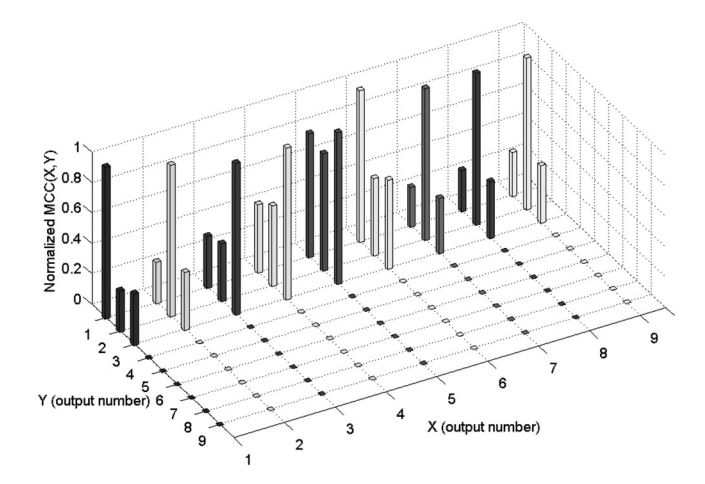


Fig. 13. Output characterization for Scenario B which shows that signals 1, 2, 3 are associated with the main paths.

We address our MCC-based selection combining approach to characterize the main source signals. In Fig. 9(a), the normalized MCC between every pair of the separated outputs is plotted. Normalized MCC is independent of the magnitude of its input signals. This feature makes normalized MCC suitable for characterization of BSS output signals. This figure confirms that MCC values of signals 1, 2, and 3 are maximum among

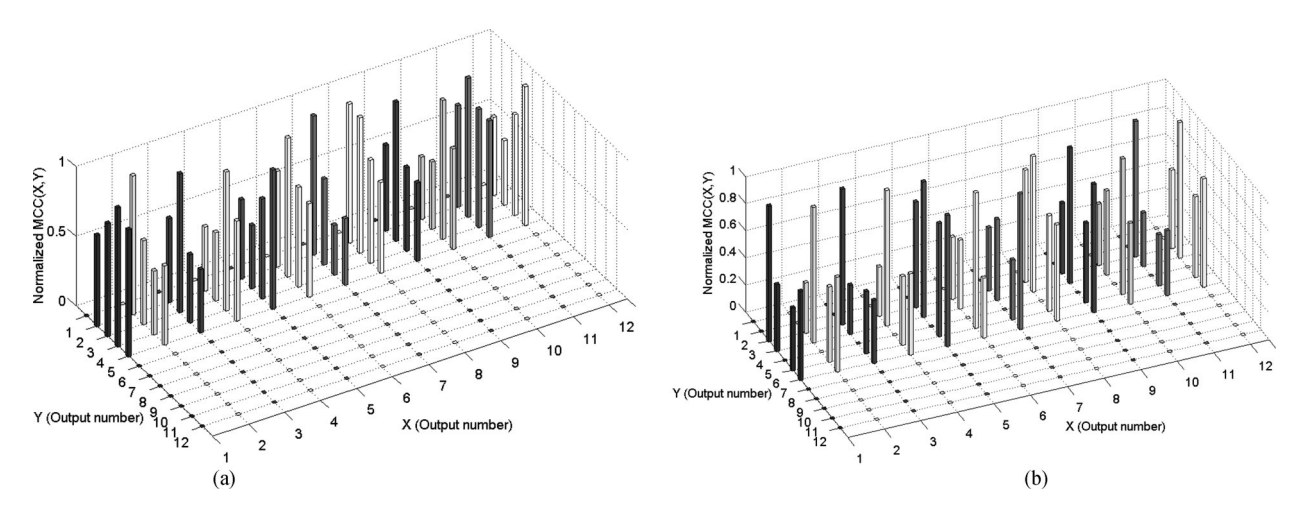


Fig. 14. (a) Output characterization for Scenario C when pilot is in location I. This figure represents signals 2, 3, 4, 5 as the main paths. (b) Characterization for Scenario C when pilot is transmitted from location II. The main signals are determined by signals 3, 4, 6, and 7.

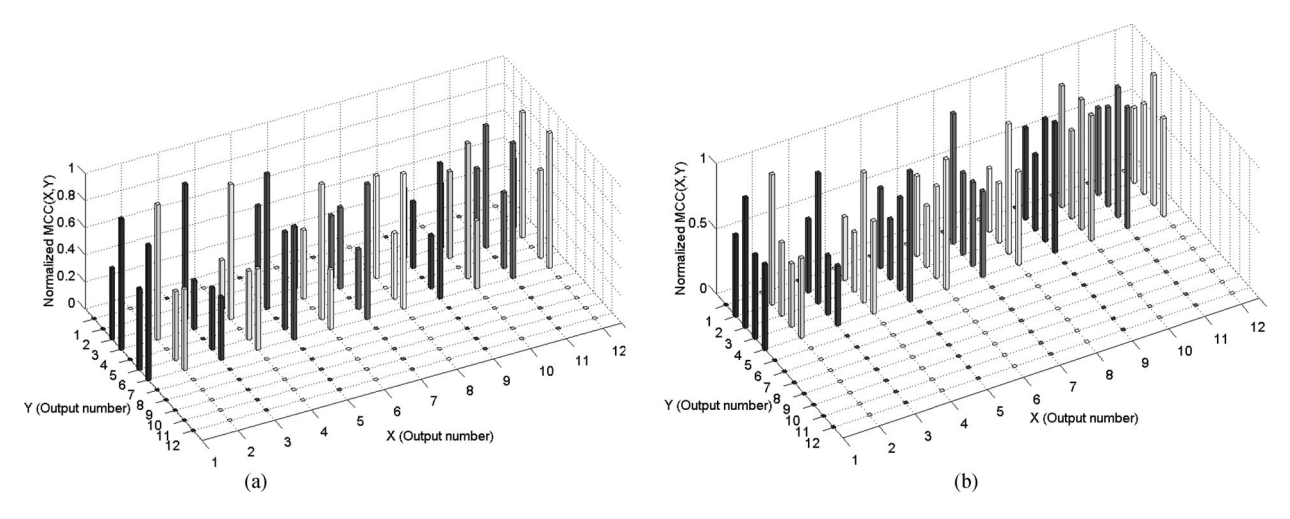


Fig. 15. (a) Output characterization for Scenario C considering pilot is emitted from location III. Signals 3, 4, 6, and 7 are associated with the main paths. (b) Characterization for Scenario C under the assumption that pilot is sent out from location IV. Signals 2, 3, 4, and 5 are determined as the main paths.

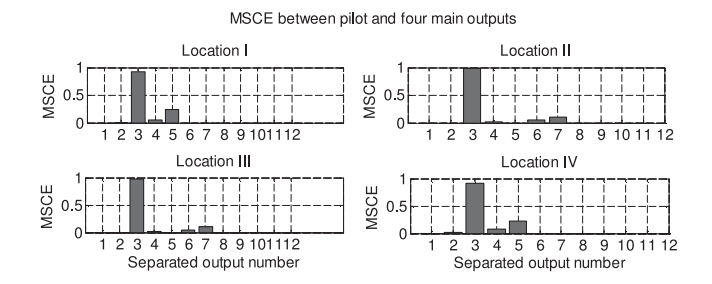


Fig. 16. Pilot identification for four different locations of pilot in Scenario C.

the others. We conclude that these signals are associated with the main paths coming from three sources. The MCC values of other signals are very low in comparison with the main signals by order of 10^{-5} . Pilot identification is executed via MSCE between these signals and the pilot. Fig. 9(b) confirms that the output number 3 with the maximum MSCE value is the separated pilot signal, since it passes both the error and reliability tests, mentioned in (17d) and (17e). Therefore, the fitting condition in (17c) is satisfied.

After distinguishing the pilot signal among the main separated signals, we wish to classify the other main outputs to one of the underwater noise class libraries. Note that according to what we defined in (10), the separated signals are $\tilde{s}_{np}(t) = s_n(t - \tau_{np})$. However, as discussed in Section III, we perform MSCE as (18), which calculates the coherency between PSD of the outputs. Therefore, the value of delays τ_{np} do not affect the classification. Fig. 10 shows PSD of the outputs in scenario A. We also provide PSD of five underwater noise sources and the pilot signal. Comparison shows that the outputs' PSDs are mostly similar to wave and shipping noise PSDs. In Fig. 11, we show and plot the coherency between outputs' PSDs and noise classes. It is depicted that output signals 1 and 2 can be classified as wave and shipping noise sources, respectively.

B. Scenario B: Multipath Effect

In this scenario, we investigate the effect of mulipath on the performance of our proposed system. We consider the same number of sources as in scenario A; however, we examine

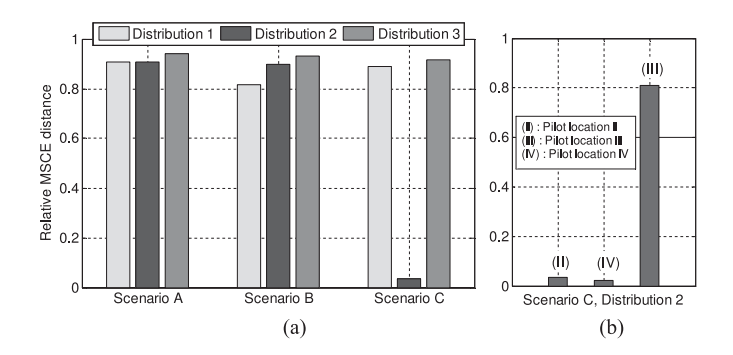


Fig. 17. (a) Relative distance Ψ_D for different distributions of sources in three defined scenarios. Distribution 1 stands for a uniform and sparse distribution, distribution 2 represents an integrated and unbalanced distribution, distribution 3 is also a sparse one while the sources are far from buoys; (b) Ψ_D for different pilot locations in Scenario C, distribution 2.

UNISeC in a three-path channel with nine active hydrophone. BSS outputs are nine signals plotted in Fig. 12(a)–(c). Fig. 13 shows MCC between every pair of separated outputs and verifies that the output signals 1, 2, and 3 are associated with the main paths. To identify the pilot signal, the algorithm calculates MSCE between pilot and three separated outputs, and the result is shown in Fig. 12(d). It is concluded that UNISeC is able to separate the signals and to characterize them in a multipath channel with larger number of paths, since signal 1 satisfies both error and reliability tests.

C. Scenario C: Traffic and Distribution Effects

Let us assume that there are three dominant noise sources in a three-path channel. We investigate execution of the algorithm in which the pilot signal is transmitted from four different locations as listed in Table I. In location I, which is the initial location in the experiment, pilot is transmitted from the sink buoy placed at the center of grid. In locations II and III, pilot is transmitted from the buoy which is close to one of the sources, and the last location considers the case that the pilot is transmitted from a buoy far from all sources. The results of characterization of main sources are shown in Figs. 14 and 15. Pilot identification is presented in Fig. 16, where error and reliability tests were satisfied. All locations have fitting index $\varpi = 1$ and total fitting index equals $\varpi_T = 0.9484$. It is apparent that UNISeC is able to separate, characterize, and identify the signals in all pilot locations.

We investigate how distribution of the sources affects the performance of UNISeC. Fig. 17(a) compares the results of the relative distance for three distributions of noise sources, for all the defined scenarios. Distribution 1 stands for a uniform and sparse distribution, distribution 2 represents an integrated and unbalanced distribution of sources, and distribution 3 is also a sparse one but noise sources are far from buoys. As shown in this figure, UNISeC passes the reliability test in all the distributions, except in Scenario C, distribution 2. However, pilot circulation can find at least one location in which UNISeC is reliable. This result is shown in Fig. 17(b). Note that in reality we deal with unknown number of sources with unknown distribution in the

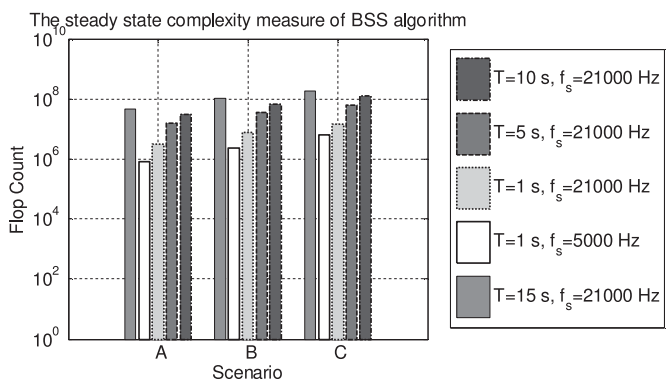


Fig. 18. Computational complexity of the proposed system in different scenarios in the steady-state phase.

ocean, so we proposed pilot circulation in UNISeC to overcome the issues such as what occurred in this simulation.

Fig. 18 compares NFP for different time periods and sampling rates in three discussed scenarios. It shows that the computational complexity increases in heavier traffic; however, UNISeC algorithm converges with different time periods and sampling rates, even under a heavy traffic and in a multipath channel.

V. CONCLUSION

Human-generated acoustic noise has increased significantly over the past decade with the increase in the use of underwater communications and the marine industry. In this work, we studied the problem of separation and classification of humangenerated or natural underwater acoustic-noise sources in a comprehensive system called UNISeC. We presented a Gray-box model and an algorithm, based on BSS, to separate the dominant sources. We also characterized and classified the separated signals. Several scenarios were considered under varying degrees of multipath, a pilot-aided probing method was exploited, and a correlation-based characterization as well as a PSD-based classification were studied.

REFERENCES

- M. Rahmati, P. Pandey, and D. Pompili, "Separation and classification of underwater acoustic sources," in *Proc. IEEE Underwater Commun. Netw.* Conf., Sestri Levante (La Spezia), Italy, 2014, pp. 1–5.
- [2] I. F. Akyildiz, D. Pompili, and T. Melodia, "Underwater acoustic sensor networks: Research challenges," *Ad Hoc Netw.*, vol. 3, no. 3, pp. 257–279, May 2005.
- [3] M. Chitre, S. Shahabudeen, and M. Stojanovic, "Underwater acoustic communications and Networking: Recent advances and future challenges," *Marine Technol. Soc. J.*, vol. 42, no. 1, pp. 103–116, 2008.
- [4] J. Imam, "Deepest part of the World's ocean is incredibly noisy scientists say," CNN, Mar. 5, 2016. [Online]. Available: http://www.cnn.com/2016/03/05/world/deep-sea-audio-recording/index.html
- [5] A. Mahmood and M. Chitre, "Modeling colored impulsive noise by Markov chains and alpha-stable processes," in *Proc. IEEE OCEANS Conf.*, Genoa, Italy, 2015, pp. 1–7.
- [6] J. Gordon et al., "A review of the effects of seismic surveys on marine mammals," Marine Technol. Soc. J., vol. 37, no. 4, pp. 16–34, 2003.
- [7] Committee on Potential Impacts of Ambient Noise in the Ocean on Marine Mammals, National Research Council, Ocean Studies Board, Division on Earth and Life Studies, *Ocean Noise and Marine Mammals*. Washington, DC. USA: National Academy Press, 2003.
- [8] R. P. Hodges, Underwater Acoustics: Analysis, Design, and Performance of Sonar. Hoboken, NJ, USA: Wiley, 2011.

- [9] W. J. Richardson, C. R. Greene, Jr., C. I. Malme, and D. H. Thomson, Marine Mammals and Noise. New York, NY, USA: Academic, 2013.
- [10] B. Chen and D. Pompili, "QUO VADIS: QoS-aware underwater optimization framework for inter-vehicle communication using acoustic directional transducers," in *Proc. IEEE Conf. Sensor, Mesh Ad Hoc Commun. Netw.*, Salt Lake City, UT, USA, Jun. 2011, pp. 341–349.
- [11] F. W. Machell, C. S. Penrod, and G. E. Ellis, Statistical Characteristics of Ocean Acoustic Noise Processes. New York, NY, USA: Springer-Verlag, 1989
- [12] G. M. Wenz, "Acoustic ambient noise in the ocean: Spectra and sources," J. Acoust. Soc. Amer., vol. 34, no. 12, pp. 1936–1956, 2005.
- [13] K. Hamed and A. R. Rao, Flood Frequency Analysis. Boca Raton, FL, USA: CRC Press, 2010.
- [14] J. A. Goldbogen et al., "Blue whales respond to simulated mid-frequency military sonar," Roy. Soc. Lond., Biol. Sci., vol. 280, no. 1765, 2013, paper no. 20130657.
- [15] C. Erbe, R. Williams, D. Sandilands, and E. Ashe, "Identifying modeled ship noise hotspots for marine mammals of Canada's pacific region," *PLoS One J.*, vol. 9, no. 3, 2014, Art. no. e89820.
- [16] S. Robinson, P. Lepper, and R. Hazelwood, "Good practice guide for underwater noise measurement," Nat. Meas. Office, Marine Scotland, The Crown Estate, 2014.
- [17] C. Gervaise, S. Vallez, C. Ioana, Y. Stéphan, and Y. Simard, "Passive acoustic Tomography: New concepts and applications using marine Mammals: A review," J. Marine Biol. Assoc. United Kingdom, vol. 87, no. 1, pp. 5–10, 2007
- [18] A. K. Morozov and D. C. Webb, "A sound projector for acoustic tomography and global ocean monitoring," *IEEE J. Ocean. Eng.*, vol. 28, no. 2, pp. 174–185, Apr. 2003.
- [19] T. Yucek and H. Arslan, "A survey of spectrum sensing algorithms for cognitive radio applications," *IEEE Commun. Surveys Tuts.*, vol. 11, no. 1, pp. 116–130, First Quarter 2009.
- [20] D. Cabric, S. M. Mishra, and R. W. Brodersen, "Implementation issues in spectrum sensing for cognitive radios," in *Proc. IEEE Asilomar Conf. Signals, Syst. Comput.*, 2004, vol. 1, pp. 772–776.
- [21] N. Baldo, P. Casari, and M. Zorzi, "Cognitive spectrum access for underwater acoustic communications," in *Proc. IEEE Int. Conf. Commun. Workshops*, 2008, pp. 518–523.
- [22] M. P. Johnson and P. L. Tyack, "A digital acoustic recording tag for measuring the response of wild marine mammals to sound," *IEEE J. Ocean. Eng.*, vol. 28, no. 1, pp. 3–12, Jan. 2003.
- [23] L. Parra and P. Sajda, "Blind source separation via generalized eigenvalue decomposition," J. Mach. Learn. Res., vol. 4, pp. 1261–1269, Dec. 2003.
- [24] S. Haykin and Z. Chen, "The cocktail party problem," *Neural Comput.*, vol. 17, no. 9, pp. 1875–1902, 2005.
- [25] A. Belouchrani, K. Abed-Meraim, J.-F. Cardoso, and E. Moulines, "A blind source separation technique using second-order statistics," *IEEE Trans. Signal Process.*, vol. 45, no. 2, pp. 434–444, Feb. 1997.
- [26] J.-F. Cardoso and A. Souloumiac, "Blind beamforming for non-Gaussian signals," *Proc. Inst. Elect. Eng., Radar Signal Process.*, vol. 140, no. 6, pp. 362–370, Dec. 1993.
- [27] J. Liu, J. Xin, and Y. Qi, "A dynamic algorithm for blind separation of convolutive sound mixtures," *Neurocomputing*, vol. 72, no. 1, pp. 521–532, 2008.
- [28] M. B. Gur and C. Niezrecki, "A source separation approach to enhancing marine mammal vocalizations," *J. Acoust. Soc. Amer.*, vol. 126, no. 6, pp. 3062–3070, 2009.
- [29] O. A. Godin, N. A. Zabotin, and V. V. Goncharov, "Ocean tomography with acoustic daylight," *Geophys. Res. Lett.*, vol. 37, no. 13, 2010, Art. no. L13605.
- [30] M.-P. Hosseini, H. Soltanian-Zadeh, K. Elisevich, and D. Pompili, "Cloud-based deep learning of big EEG data for epileptic seizure prediction," in *Proc. IEEE Global Conf. Signal Inf. Process.*, Washington, DC, USA, 2016, pp. 1151–1155.
- [31] A. Hajisami, H. Viswanathan, and D. Pompili, "Cocktail party in the cloud: Blind source separation for co-operative cellular communication in cloud RAN," in *Proc. IEEE Conf. Mobile Ad Hoc Sensor Syst.*, 2014, pp. 37–45.
- [32] P. van Walree, "Propagation and scattering effects in underwater acoustic communication channels," *IEEE J. Ocean. Eng.*, vol. 38, no. 4, pp. 614–631, Oct. 2013.
- [33] L. M. Brekhovskikh, Fundamentals of Ocean Acoustics. New York, NY, USA: Springer-Verlag, 2003.

- [34] M. Stojanovic and J. Preisig, "Underwater acoustic communication Channels: Propagation models and statistical characterization," *IEEE Commun. Mag.*, vol. 47, no. 1, pp. 84–89, Jan. 2009.
- [35] M. Stojanovic, "On the relationship between capacity and distance in an underwater acoustic communication channel," ACM SIGMOBILE Mobile Comput. Commun. Rev., vol. 11, no. 4, pp. 34–43, 2007.
- [36] P. Qarabaqi and M. Stojanovic, "Statistical characterization and computationally efficient modeling of a class of underwater acoustic communication channels," *IEEE J. Ocean. Eng.*, vol. 38, no. 4, pp. 701–717, Oct. 2013.
- [37] M. Porter *et al.*, "Bellhop code," Acoustics Toolbox, 2013. [Online]. Available: http://oalib.hlsresearch.com/Rays
- [38] P. Comon and C. Jutten, Handbook of Blind Source Separation: Independent Component Analysis and Applications. New York, NY, USA: Academic, 2010.
- [39] G. H. Golub and C. F. Van Loan, *Matrix Computations*, vol. 3. Baltimore, MD, USA: The Johns Hopkins Univ. Press, 2012.
- [40] T. P. Bohlin, Practical Grey-Box Process Identification: Theory and Applications, 1st ed. New York, NY, USA: Springer-Verlag, 2010.
- [41] G. C. Carter, "Coherence and time delay estimation," *Proc. IEEE*, vol. 75, no. 2, pp. 236–255, Feb. 1987.
- [42] J. Mann, Cetacean Societies: Field Studies of Dolphins and Whales. Chicago, IL, USA: Univ. of Chicago Press, 2000.
- [43] G. R. Naik and W. Wang, Blind Source Separation: Advances in Theory, Algorithms and Applications. New York, NY, USA: Springer-Verlag, 2014.



Mehdi Rahmati (S'15) received the B.S. degree in electrical engineering from Ferdowsi University of Mashhad, Mashhad, Iran, in 2001 and the M.S. degree in communications and electrical engineering from Iran University of Science and Technology, Tehran, Iran, in 2009. He is currently working toward the Ph.D. degree in the Department of Electrical and Computer Engineering, Rutgers University, New Brunswick, NJ, USA, under Prof. D. Pompili in the Cyber-Physical Systems Laboratory.

He was a full-time faculty member at Bahar Institute of Higher Education and a Lecturer at Azad University of Tehran and Mashhad, both in Iran. For his M.S. thesis, he worked on MIMO coding in correlated wireless channels; currently, he is working on underwater acoustic communications and networks.



Dario Pompili (SM'14) received the *Laurea* (combined B.S. and M.S.) and Doctorate degrees in telecommunications and system engineering from the University of Rome "La Sapienza," Rome, Italy, in 2001 and 2004, respectively, and the Ph.D. degree in electrical and computer engineering (ECE) from Georgia Institute of Technology, Atlanta, GA, USA, in June 2007.

He is currently an Associate Professor with the Department of ECE, Rutgers University, New Brunswick, NJ, USA. He is also the Director of the

Cyber-Physical Systems Laboratory (CPS Lab), which focuses on mobile computing, wireless communications and networking, acoustic communications, sensor networks, and data center management. He published more than a hundred refereed scholar publications, with almost 7000 citations.

Dr. Pompili received the NSF CAREER'11 Award, the ONR Young Investigator Program'12 Award, and the DARPA Young Faculty'12 Award. In 2015, he was nominated Rutgers-New Brunswick Chancellor's Scholar. He has an h-index of 29 and a i10-index of 52 (Google Scholar, May'17). Since 2014, he has been a Senior Member of both the IEEE Communications Society and the ACM